

H2S AND CO2 CORROSION OF SA-543 AND X65 STEELS IN OIL /WATER EMULSION	العنوان:
Zafar, Muhammad Nauman	المؤلف الرئيسي:
Al Hadhrami, Luai Muhammad, Rihan, Rihan O.(Advisor, Co-Advisor)	مؤلفين آخرين:
2014	التاريخ الميلادي:
الظهران	موقع:
1 - 121	الصفحات:
651787	رقم MD:
رسائل جامعية	نوع المحتوى:
English	اللغة:
رسالة ماجستير	الدرجة العلمية:
جامعة الملك فهد للبترول والمعادن	الجامعة:
عمادة الدراسات العليا	الكلية:
السعودية	الدولة:
Dissertations	قواعد المعلومات:
التآكل، الصلابة، الهندسة الميكانيكية	مواضيع:
<a href="https://search.mandumah.com/Record/651787">https://search.mandumah.com/Record/651787</a>	رابط:

## ABSTRACT

**Full Name : Muhammad Nauman Zafar**

**Thesis title : H<sub>2</sub>S and CO<sub>2</sub> corrosion of SA-543 and X65 steels in oil/water emulsion corrosion**

**Major Field : Mechanical Engineering**

**Date of Degree : March, 2014**

An experimental study was performed using rotating cylinder electrode and a novel emulsion flow loop to investigate the corrosion behaviour of SA-543 and X65 steels when exposed to emulsion containing oil and sodium thiosulphate (Na<sub>2</sub>S<sub>2</sub>O<sub>3</sub>) solution along with carbon dioxide (CO<sub>2</sub>). This study aimed at understanding the effects of hydrodynamics on corrosion. Na<sub>2</sub>S<sub>2</sub>O<sub>3</sub> was used to generate the hydrogen sulphide (H<sub>2</sub>S). The emulsions were formed using 0.01 M Na<sub>2</sub>S<sub>2</sub>O<sub>3</sub> and Exxsol D80 oil. To mimic the well conditions, CO<sub>2</sub> was purged in order to maintain a pH of 5. Experiments were performed for different ranges of oil content, velocity, temperature, viscosity, and pipe diameter. Individual and combined effects of thiosulphate and CO<sub>2</sub> were also studied. It was observed that SA-543 steel was more corrosion resistant than X65 steel in the emulsion solution. Similar corrosion trend was found for both RCE and flow loop under the same test conditions. Iron sulphide film was formed on all the samples. Corrosion rates were reduced upon the introduction of CO<sub>2</sub> in the flowing fluid. The presence of oily phase dwindled the corrosion due to its inertness as oil is adsorbed on the steel surface. Increasing the velocity augmented the kinetics of reduction reaction thus forming sulphide film at higher rate and hence inhibiting the corrosion. Varying the temperature had a similar effect; corrosion dwindled by increasing the temperature due to the formation of stable sulphide films that are formed at higher temperatures. The corrosion

## الخلاصة

الاسم: محمد نعمان ظفر

عنوان الرسالة: تسبب كبريتيد الهيدروجين وثنائي أكسيد الكربون في تآكل الفولاذ SA-543 و X65 في المستحلبات المائية / النفطية

التخصص الرئيسي: الهندسة الميكانيكية

تاريخ الدرجة العلمية: مارس 2014

تم إجراء دراسة تجريبية باستخدام قطب اسطواني دوار و جهاز تدفق حلقي جديد لم يتم استخدامه من قبل لدراسة سلوك تآكل الفولاذ SA-543 و X65 ، عند التعرض لمستحلب يحتوي على النفط ومحلول ثيوكبريتات الصوديوم ( $Na_2S_2O_3$ ) بالإضافة إلى ثاني أكسيد الكربون ( $CO_2$ ). وتهدف هذه الدراسة فهم آثار قوى الموائع على التآكل. وقد استخدم ثيوكبريتات الصوديوم لتوليد كبريتيد الهيدروجين ( $H_2S$ ). وتم تشكيل المستحلبات باستخدام 0.01 مل من ثيوكبريتات الصوديوم ( $Na_2S_2O_3$ ) ، و الزيت Exxsol D80. ولمحاكاة ظروف البئر تم إضافة ثاني أكسيد الكربون ( $CO_2$ ) من أجل الحفاظ على درجة 5 للأس الهيدروجيني. وقد أجريت التجارب على نطاقات مختلفة من محتوى الزيت ، والسرعة ، ودرجة الحرارة ، واللزوجة ، وقطر الأنبوب. وقد تم أيضا دراسة التأثير الفردي و الجماعي للثيوكبريتات وثنائي أكسيد الكربون. ولوحظ أن فولاذ SA-543 كان أكثر مقاومة للتآكل من فولاذ X65 في محلول المستحلب. وقد تبين وجود نفس سلوك التآكل في كل من القطب الاسطواني الدوار و جهاز التدفق الحلقي في ظل نفس ظروف الإختبار. وتشكلت طبقة من كبريتيد الحديد على جميع العينات. وظهر تثبيط أكثر في عملية التآكل في التجارب التي تم إضافة ثاني أكسيد الكربون إليها. و أدى وجود الزيت إلى تضاءل التآكل بسبب وجود طبقة من الزيت على سطح الفولاذ. وتسببت زيادة السرعة في زيادة حركية تفاعل الاختزال وبالتالي تشكلت طبقة من الكبريتيد بمعدل أعلى مما ثبت التآكل. وقد كان لتغيير درجة الحرارة تأثير مماثل ، حيث تضاءل التآكل مع زيادة درجة الحرارة بسبب تشكل طبقات مستقرة من الكبريتيد والتي تتشكل عند درجات الحرارة العالية. وكان معدل التآكل في العينة الموجودة بالقرب من مدخل قناة الإختبار أكثر من العينة الموجودة بالقرب من مخرج قناة الإختبار بسبب زيادة الاضطرابات التدفقية عند المدخل. وأدت الزيادة في لزوجة النفط إلى الزيادة في معدل التآكل وذلك بسبب ارتفاع إجهادات القص.

## درجة الماجستير في العلوم

جامعة الملك فهد للبترول والمعادن

الظهران - المملكة العربية السعودية

H2S AND CO2 CORROSION OF SA-543 AND X65 STEELS IN OIL /WATER EMULSION	العنوان:
Zafar, Muhammad Nauman	المؤلف الرئيسي:
Al Hadhrami, Luai Muhammad, Rihan, Rihan O.(Advisor, Co-Advisor)	مؤلفين آخرين:
2014	التاريخ الميلادي:
الظهران	موقع:
1 - 121	الصفحات:
651787	رقم MD:
رسائل جامعية	نوع المحتوى:
English	اللغة:
رسالة ماجستير	الدرجة العلمية:
جامعة الملك فهد للبترول والمعادن	الجامعة:
عمادة الدراسات العليا	الكلية:
السعودية	الدولة:
Dissertations	قواعد المعلومات:
التآكل، الصلابة، الهندسة الميكانيكية	مواضيع:
<a href="https://search.mandumah.com/Record/651787">https://search.mandumah.com/Record/651787</a>	رابط:

## TABLE OF CONTENTS

<b>ACKNOWLEDGEMENT</b> .....	<b>v</b>
<b>TABLE OF CONTENTS</b> .....	<b>vi</b>
<b>LIST OF FIGURES</b> .....	<b>viii</b>
<b>LIST OF TABLES</b> .....	<b>xii</b>
<b>LIST OF ABBREVIATIONS</b> .....	<b>xiii</b>
<b>ABSTRACT</b> .....	<b>xiv</b>
<b>ABSTRACT ARABIC</b> .....	<b>xvi</b>
<b>CHAPTER 1 INTRODUCTION</b> .....	<b>1</b>
1.1 Introduction .....	1
1.2 Thesis objective.....	6
1.3 Thesis structure .....	6
<b>CHAPTER 2 LITERATURE REVIEW</b> .....	<b>7</b>
2.1 Literatures.....	7
2.1.1 H <sub>2</sub> S and CO <sub>2</sub> corrosion .....	7
2.1.2 Rotating Cylinder.....	13
2.1.3 Flow Loop.....	18
2.2 University Research .....	23
2.3 Research Motivation .....	24
<b>CHAPTER 3 EXPERIMENTAL APPARATUS</b> .....	<b>25</b>
3.1 Rotating cylinder electrode .....	25
3.1.1 Experimental setup.....	25
3.1.2 Procedure .....	26
3.1.3 Data reduction .....	30
3.2 Novel emulsion flow loop.....	32
3.2.1 Experimental setup.....	32
3.2.2 Procedure .....	56
3.2.3 Data reduction .....	64

3.3	Test material .....	66
3.3.1	Test area of RCE .....	68
3.3.2	Test area for flow loop .....	68
<b>CHAPTER 4 RESULTS AND DISSCUSSIONS .....</b>		<b>71</b>
4.1	Rotating cylinder electrode .....	71
4.1.1	Effect of Na <sub>2</sub> S <sub>2</sub> O <sub>3</sub> , CO <sub>2</sub> and NaCl .....	71
4.1.2	Emulsion at different oil percentages .....	78
4.1.3	Effect of Velocities .....	82
4.1.4	Effect of Temperature .....	85
4.2	Flow loop .....	88
4.2.1	Effect of CO <sub>2</sub> emulsion corrosion .....	88
4.2.2	Emulsion at different oil percentages .....	92
4.2.3	Effect of velocity on corrosion .....	95
4.2.4	Effect of temperature on corrosion .....	98
4.2.5	Corrosion behaviour along the pipe length with D80 oil .....	101
4.2.6	Effect of oil viscosity on corrosion .....	105
<b>CHAPTER 5 CONCLUSIONS AND RECOMMENDATIONS .....</b>		<b>109</b>
5.1	Conclusion .....	109
5.1.1	Rotating Cylinder Electrode .....	109
5.1.2	Flow Loop .....	110
5.2	Recommendation .....	111
<b>REFERENCES .....</b>		<b>112</b>
<b>VITAE .....</b>		<b>120</b>

## LIST OF FIGURES

Figure 3.1 Rotating shaft with working samples and impeller. ....	28
Figure 3.2 The experimental apparatus.....	29
Figure 3.3 Emulsion flow loop. ....	33
Figure 3.4 Flow loop front view. ....	35
Figure 3.5 Flow loop test sections. ....	36
Figure 3.6 Electrodes positioning in test section. ....	37
Figure 3.7 Test sections dimensions in mm.....	38
Figure 3.8 Preparation tank and mixer.....	40
Figure 3.9 Autoclave.....	41
Figure 3.10 Pumps. ....	44
Figure 3.11 Dosing Pumps.....	44
Figure 3.12 pH chamber. ....	45
Figure 3.13 pH probe. ....	46
Figure 3.14 Control panel. ....	47
Figure 3.15 Flow meters. ....	48
Figure 3.16 A detailed drawing of the sample/specimen holder. ....	52
Figure 3.17 The electrode surface through a cross section of a test section. ....	52
Figure 3.18 Potentiostat. ....	53
Figure 3.19 Multiplexer. ....	54
Figure 3.20 Reference chamber. ....	55
Figure 3.21 A diagram illustrating the direction the flow (front view). ....	58
Figure 3.22 A diagram illustrating the direction the flow (top view). ....	59

Figure 3.23	A photograph illustrating the direction the flow (top view).....	60
Figure 3.24	A photograph illustrating the direction the flow in the primary circulating loop. ....	61
Figure 3.25	Piping and instrumentation diagram (PID) of emulsion flow loop. ....	62
Figure 3.26	Milky emulsion in transparent pipe.....	63
Figure 3.27	The microstructure of SA-543 steel. ....	67
Figure 3.28	The microstructure of X-65 steel.....	67
Figure 3.29	Sample mounting.....	69
Figure 3.30	Diagram to calculate exposed electrode area. ....	70
Figure 4.1	The potentiodynamic polarization curves of SA-543 and X65 steels in 0.01 M $\text{Na}_2\text{S}_2\text{O}_3$ solution with 30% oil at 1 m/s, and 25°C after 24 hours. ....	73
Figure 4.2	Polarization resistance of SA-543 and X65 steels with time in 0.01 M $\text{Na}_2\text{S}_2\text{O}_3$ solution with 30% oil at 1 m/s, and 25°C. ....	75
Figure 4.3	Corrosion rate measurement of SA-543 and X65 steels using the weight loss method in 0.01 M $\text{Na}_2\text{S}_2\text{O}_3$ solution with 30 % oil at 25°C and 1 m/s.....	77
Figure 4.4	The potentiodynamic polarization curves of SA-543 steel in different oil percentages with 0.01 M $\text{Na}_2\text{S}_2\text{O}_3$ solution at 25°C and 1 m/s. ....	80
Figure 4.5	Polarization resistance of SA-543 steel with time in 0.01 M $\text{Na}_2\text{S}_2\text{O}_3$ solution with 30% oil at different oil percentages.....	80
Figure 4.6	Corrosion rate measurement of SA-543 steel at different oil concentrations using the weight loss method. ....	81
Figure 4.7	The potentiodynamic polarization curves of SA-543 steel in 0.01 M $\text{Na}_2\text{S}_2\text{O}_3$ solution with 30% oil at 25°C and different velocities.....	83



Figure 4.8	$R_p$ of SA-543 steel with time in 0.01 M $\text{Na}_2\text{S}_2\text{O}_3$ solution with 30% oil at 25°C and different velocities. ....	83
Figure 4.9	Corrosion rate measurement of SA-543 steel at different velocities using the weight loss method. ....	84
Figure 4.10	The potentiodynamic polarization curves of SA-543 steel in 0.01 M $\text{Na}_2\text{S}_2\text{O}_3$ solution with 30% oil at 1 m/s and different temperatures.....	86
Figure 4.11	$R_p$ of SA-543 steel with time in 0.01 M $\text{Na}_2\text{S}_2\text{O}_3$ solution with 30% oil at 1 m/s and different temperatures.....	86
Figure 4.12	Corrosion rate measurement of SA-543 steel at 1 m/s and different temperatures using the weight loss method.....	87
Figure 4.13	The potentiodynamic polarization curves of SA-543 and X65 steels in 0.01 M $\text{Na}_2\text{S}_2\text{O}_3$ solution with 30% oil at 1 m/s and 25°C.....	89
Figure 4.14	$R_p$ of SA-543 and X65 steels with time in 0.01 M $\text{Na}_2\text{S}_2\text{O}_3$ solution with 30% oil at 1 m/s and 25°C. ....	91
Figure 4.15	Corrosion rate measurement of SA-543 and X65 steels in 0.01 M $\text{Na}_2\text{S}_2\text{O}_3$ solution with 30 % oil at 25°C and 1 m/s.....	91
Figure 4.16	The potentiodynamic polarization curves of SA-543 steel in different oil percentages with 0.01 M $\text{Na}_2\text{S}_2\text{O}_3 + \text{CO}_2$ solution at 25°C and 1 m/s.....	93
Figure 4.17	$R_p$ of SA-543 steel with time in 0.01 M $\text{Na}_2\text{S}_2\text{O}_3 + \text{CO}_2$ solution at different oil percentages. ....	93
Figure 4.18	Corrosion rate measurement of SA-543 and X65 steels at different oil percentages. ....	94

Figure 4.19	The potentiodynamic polarization curves of SA-543 steel in 0.01 M Na <sub>2</sub> S <sub>2</sub> O <sub>3</sub> + CO <sub>2</sub> solution with 30% oil at 25°C and different velocities. ....	96
Figure 4.20	R <sub>p</sub> of SA-543 steel with time in 0.01 M Na <sub>2</sub> S <sub>2</sub> O <sub>3</sub> + CO <sub>2</sub> solution with 30% oil at 25°C and different velocities.....	97
Figure 4.21	Corrosion rate measurement of SA-543 steel at different velocities.....	97
Figure 4.22	The potentiodynamic polarization curves of SA-543 steel in 0.01 M Na <sub>2</sub> S <sub>2</sub> O <sub>3</sub> + CO <sub>2</sub> solution with 30% oil at 1 m/s and different temperatures. ....	99
Figure 4.23	R <sub>p</sub> of SA-543 steel with time in 0.01 M Na <sub>2</sub> S <sub>2</sub> O <sub>3</sub> + CO <sub>2</sub> solution with 30% oil at 1 m/s and different temperatures. ....	99
Figure 4.24	Corrosion rate measurement of SA-543 steel at 1 m/s and different temperatures. ....	100
Figure 4.25	Vena contracta demonstration. ....	102
Figure 4.26	The potentiodynamic polarization curve for Exxsol D80 oil at 30% Oil and 70 % 0.01 M Na <sub>2</sub> S <sub>2</sub> O <sub>3</sub> . ....	103
Figure 4.27	Corrosion rate trend for Exxsol D80 oil at 30% Oil and 70% 0.01 M Na <sub>2</sub> S <sub>2</sub> O <sub>3</sub> . ....	103
Figure 4.28	Corrosion rate of D80 oil at different electrode positions. ....	104
Figure 4.29	The potentiodynamic polarization curve for Exxsol D80 and D130 oils at 30% Oil and 70% 0.01 M Na <sub>2</sub> S <sub>2</sub> O <sub>3</sub> . ....	106
Figure 4.30	Corrosion rate trend for Exxsol D80 and D130 oils at 30% Oil and 70% 0.01 M Na <sub>2</sub> S <sub>2</sub> O <sub>3</sub> . ....	108
Figure 4.31	Corrosion rate of D80 and D130 oils at different electrode positions.....	108

## LIST OF TABLES

Table 3.1 Chemical and physical properties of Exxsol D80 and D130 oils. ....	31
Table 3.2 Pumps specification. ....	43
Table 3.3 Flow-meter specification. ....	49
Table 3.4 Chemical Composition of SA-543 and X65 steels. ....	66
Table 3.5 Exposed area of test electrodes in different test sections. ....	70
Table 4.1 Tafel extrapolation data. ....	72
Table 4.2 Experimental series chart. ....	78
Table 4.3 Tafel extrapolation for different oil percentages ....	79
Table 4.4 Tafel extrapolation for different velocities. ....	82
Table 4.5 Tafel extrapolation for different temperatures. ....	85
Table 4.6 Tafel extrapolation for Na <sub>2</sub> S <sub>2</sub> O <sub>3</sub> and CO <sub>2</sub> . ....	89
Table 4.7 Tafel extrapolation for different oil percentages ....	92
Table 4.8 Tafel extrapolation for different velocities. ....	96
Table 4.9 Tafel extrapolation for different temperatures. ....	98
Table 4.10 Tafel extrapolation along the pipe length. ....	102
Table 4.11 Tafel extrapolation for different oils. ....	105

## LIST OF ABBREVIATIONS

$I_{\text{corr}}$	:	Corrosion current
$E_{\text{corr}}$	:	Corrosion potential
$\beta_a$	:	Anodic Tafel constant
$\beta_c$	:	Cathodic Tafel constant
$\text{Na}_2\text{S}_2\text{O}_3$	:	Sodium thiosulphate
$\text{CO}_2$	:	Carbon dioxide
O/W	:	Oil-in-water emulsion
W/O	:	Water-in-oil emulsion
$\text{H}_2\text{S}$	:	Hydrogen sulphide
$R_p$	:	Polarization resistance
$J_{\text{corr}}$	:	Current density
RCE	:	Rotating cylinder electrode
FAC	:	Flow accelerated corrosion

H2S AND CO2 CORROSION OF SA-543 AND X65 STEELS IN OIL /WATER EMULSION	العنوان:
Zafar, Muhammad Nauman	المؤلف الرئيسي:
-Al Hadhrami, Luai Muhammad, Rihan, Rihan O.(Advisor, Co Advisor)	مؤلفين آخرين:
2014	التاريخ الميلادي:
الظهران	موقع:
1 - 121	الصفحات:
651787	رقم MD:
رسائل جامعية	نوع المحتوى:
English	اللغة:
رسالة ماجستير	الدرجة العلمية:
جامعة الملك فهد للبترول والمعادن	الجامعة:
عمادة الدراسات العليا	الكلية:
السعودية	الدولة:
Dissertations	قواعد المعلومات:
التآكل، الصلابة، الهندسة الميكانيكية	مواضيع:
<a href="https://search.mandumah.com/Record/651787">https://search.mandumah.com/Record/651787</a>	رابط:

**H<sub>2</sub>S AND CO<sub>2</sub> CORROSION OF SA-543 AND X65**

**STEELS IN OIL/WATER EMULSION**

BY

**MUHAMMAD NAUMAN ZAFAR**

A Thesis Presented to the  
DEANSHIP OF GRADUATE STUDIES

**KING FAHD UNIVERSITY OF PETROLEUM & MINERALS**

DHAHRAN, SAUDI ARABIA

1963 ١٣٨٣

In Partial Fulfillment of the  
Requirements for the Degree of

**MASTER OF SCIENCE**

In

**MECHANICAL ENGINEERING**


**MARCH 2014**

KING FAHD UNIVERSITY OF PETROLEUM & MINERALS

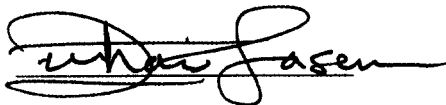
DHAHRAN- 31261, SAUDI ARABIA

DEANSHIP OF GRADUATE STUDIES

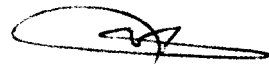
This thesis, written by **MUHAMMAD NAUMAN ZAFAR** under the direction his thesis advisor and approved by his thesis committee, has been presented and accepted by the Dean of Graduate Studies, in partial fulfilment of the requirements for the degree of **MASTER OF SCIENCE IN MECHANICAL ENGINEERING.**



Dr. Luai M. Al-Hadhrami  
(Advisor)



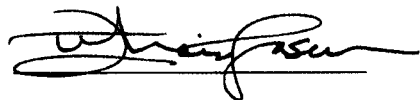
Dr. Zuhair M. A. Gasem  
Department Chairman



Dr. Rihan O. Rihan  
(Co-Advisor)



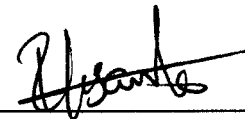
Dr. Salam A. Zummo  
Dean of Graduate Studies



Dr. Zuhair M. A. Gasem  
(Member)

15/5/14

Date



Dr. Ihsan ul Haq Toor  
(Member)



Dr. Rami K.M. Suleiman  
(Member)

© Muhammad Nauman Zafar

2014



Dedicated to my beloved parents, grandmother, brothers and my fiancé

## **ACKNOWLEDGEMENT**

First of all I would like to thank Almighty ALLAH for bestowing me strength and knowledge to undertake this research and guiding me step by step till its completion. I am grateful to my parents and brothers for their untiring support and prayers. They were a source of inspiration and continuous support for me. I would like to thank to my fiancé for being on my side and encouraging me to finish my thesis.

I would like to thank my advisor Dr. Luai Al Hadhrami and my co-advisor Dr. Rihan O. Rihan for their continuous support and encouraging me to uptake this challenge and guiding me till the end of this research. I would like to thank my committee members, Dr. Zuhair, Dr. Ihsan and Dr. Rami for their guidance in this research work.

I would like to thank all my colleagues at Center of Research Excellence in Corrosion, Research Institute. Special thanks to my roommate Farooq Riaz for bearing me for 3 years and encouraging me to complete my write up. I would like to acknowledge the support of Ahmad Rafiq, Hussain Ali, Umar Khan, Omer bin Sohail, Mudassar Imam, Amir Hamza, Khobeb Muslim, Pamir Aly and Haroon Ashraf for making this journey memorable.

Finally I would like to acknowledge the support provided by Mr. Siddiqui, Mr. Abdul Quddus, Mr. Muneer, Mr. Hatim, Mr. Lateef and Mr. Sadaqat for helping me out during my experimental work.

## TABLE OF CONTENTS

<b>ACKNOWLEDGEMENT</b> .....	<b>v</b>
<b>TABLE OF CONTENTS</b> .....	<b>vi</b>
<b>LIST OF FIGURES</b> .....	<b>viii</b>
<b>LIST OF TABLES</b> .....	<b>xii</b>
<b>LIST OF ABBREVIATIONS</b> .....	<b>xiii</b>
<b>ABSTRACT</b> .....	<b>xiv</b>
<b>ABSTRACT ARABIC</b> .....	<b>xvi</b>
<b>CHAPTER 1 INTRODUCTION</b> .....	<b>1</b>
1.1 Introduction .....	1
1.2 Thesis objective.....	6
1.3 Thesis structure .....	6
<b>CHAPTER 2 LITERATURE REVIEW</b> .....	<b>7</b>
2.1 Literatures.....	7
2.1.1 H <sub>2</sub> S and CO <sub>2</sub> corrosion .....	7
2.1.2 Rotating Cylinder.....	13
2.1.3 Flow Loop.....	18
2.2 University Research .....	23
2.3 Research Motivation .....	24
<b>CHAPTER 3 EXPERIMENTAL APPARATUS</b> .....	<b>25</b>
3.1 Rotating cylinder electrode .....	25
3.1.1 Experimental setup.....	25
3.1.2 Procedure .....	26
3.1.3 Data reduction .....	30
3.2 Novel emulsion flow loop.....	32
3.2.1 Experimental setup.....	32
3.2.2 Procedure .....	56
3.2.3 Data reduction .....	64

3.3	Test material .....	66
3.3.1	Test area of RCE .....	68
3.3.2	Test area for flow loop .....	68
<b>CHAPTER 4 RESULTS AND DISSCUSSIONS .....</b>		<b>71</b>
4.1	Rotating cylinder electrode .....	71
4.1.1	Effect of Na <sub>2</sub> S <sub>2</sub> O <sub>3</sub> , CO <sub>2</sub> and NaCl .....	71
4.1.2	Emulsion at different oil percentages .....	78
4.1.3	Effect of Velocities .....	82
4.1.4	Effect of Temperature .....	85
4.2	Flow loop .....	88
4.2.1	Effect of CO <sub>2</sub> emulsion corrosion .....	88
4.2.2	Emulsion at different oil percentages .....	92
4.2.3	Effect of velocity on corrosion .....	95
4.2.4	Effect of temperature on corrosion .....	98
4.2.5	Corrosion behaviour along the pipe length with D80 oil .....	101
4.2.6	Effect of oil viscosity on corrosion .....	105
<b>CHAPTER 5 CONCLUSIONS AND RECOMMENDATIONS .....</b>		<b>109</b>
5.1	Conclusion .....	109
5.1.1	Rotating Cylinder Electrode .....	109
5.1.2	Flow Loop .....	110
5.2	Recommendation .....	111
<b>REFERENCES .....</b>		<b>112</b>
<b>VITAE .....</b>		<b>120</b>

## LIST OF FIGURES

Figure 3.1 Rotating shaft with working samples and impeller. ....	28
Figure 3.2 The experimental apparatus.....	29
Figure 3.3 Emulsion flow loop. ....	33
Figure 3.4 Flow loop front view. ....	35
Figure 3.5 Flow loop test sections. ....	36
Figure 3.6 Electrodes positioning in test section. ....	37
Figure 3.7 Test sections dimensions in mm.....	38
Figure 3.8 Preparation tank and mixer.....	40
Figure 3.9 Autoclave.....	41
Figure 3.10 Pumps. ....	44
Figure 3.11 Dosing Pumps.....	44
Figure 3.12 pH chamber. ....	45
Figure 3.13 pH probe. ....	46
Figure 3.14 Control panel. ....	47
Figure 3.15 Flow meters. ....	48
Figure 3.16 A detailed drawing of the sample/specimen holder. ....	52
Figure 3.17 The electrode surface through a cross section of a test section. ....	52
Figure 3.18 Potentiostat. ....	53
Figure 3.19 Multiplexer. ....	54
Figure 3.20 Reference chamber. ....	55
Figure 3.21 A diagram illustrating the direction the flow (front view). ....	58
Figure 3.22 A diagram illustrating the direction the flow (top view). ....	59

Figure 3.23	A photograph illustrating the direction the flow (top view).....	60
Figure 3.24	A photograph illustrating the direction the flow in the primary circulating loop. ....	61
Figure 3.25	Piping and instrumentation diagram (PID) of emulsion flow loop. ....	62
Figure 3.26	Milky emulsion in transparent pipe.....	63
Figure 3.27	The microstructure of SA-543 steel. ....	67
Figure 3.28	The microstructure of X-65 steel.....	67
Figure 3.29	Sample mounting.....	69
Figure 3.30	Diagram to calculate exposed electrode area. ....	70
Figure 4.1	The potentiodynamic polarization curves of SA-543 and X65 steels in 0.01 M $\text{Na}_2\text{S}_2\text{O}_3$ solution with 30% oil at 1 m/s, and 25°C after 24 hours. ....	73
Figure 4.2	Polarization resistance of SA-543 and X65 steels with time in 0.01 M $\text{Na}_2\text{S}_2\text{O}_3$ solution with 30% oil at 1 m/s, and 25°C. ....	75
Figure 4.3	Corrosion rate measurement of SA-543 and X65 steels using the weight loss method in 0.01 M $\text{Na}_2\text{S}_2\text{O}_3$ solution with 30 % oil at 25°C and 1 m/s.....	77
Figure 4.4	The potentiodynamic polarization curves of SA-543 steel in different oil percentages with 0.01 M $\text{Na}_2\text{S}_2\text{O}_3$ solution at 25°C and 1 m/s. ....	80
Figure 4.5	Polarization resistance of SA-543 steel with time in 0.01 M $\text{Na}_2\text{S}_2\text{O}_3$ solution with 30% oil at different oil percentages.....	80
Figure 4.6	Corrosion rate measurement of SA-543 steel at different oil concentrations using the weight loss method. ....	81
Figure 4.7	The potentiodynamic polarization curves of SA-543 steel in 0.01 M $\text{Na}_2\text{S}_2\text{O}_3$ solution with 30% oil at 25°C and different velocities.....	83

Figure 4.8	$R_p$ of SA-543 steel with time in 0.01 M $\text{Na}_2\text{S}_2\text{O}_3$ solution with 30% oil at 25°C and different velocities. ....	83
Figure 4.9	Corrosion rate measurement of SA-543 steel at different velocities using the weight loss method. ....	84
Figure 4.10	The potentiodynamic polarization curves of SA-543 steel in 0.01 M $\text{Na}_2\text{S}_2\text{O}_3$ solution with 30% oil at 1 m/s and different temperatures.....	86
Figure 4.11	$R_p$ of SA-543 steel with time in 0.01 M $\text{Na}_2\text{S}_2\text{O}_3$ solution with 30% oil at 1 m/s and different temperatures.....	86
Figure 4.12	Corrosion rate measurement of SA-543 steel at 1 m/s and different temperatures using the weight loss method.....	87
Figure 4.13	The potentiodynamic polarization curves of SA-543 and X65 steels in 0.01 M $\text{Na}_2\text{S}_2\text{O}_3$ solution with 30% oil at 1 m/s and 25°C.....	89
Figure 4.14	$R_p$ of SA-543 and X65 steels with time in 0.01 M $\text{Na}_2\text{S}_2\text{O}_3$ solution with 30% oil at 1 m/s and 25°C. ....	91
Figure 4.15	Corrosion rate measurement of SA-543 and X65 steels in 0.01 M $\text{Na}_2\text{S}_2\text{O}_3$ solution with 30 % oil at 25°C and 1 m/s.....	91
Figure 4.16	The potentiodynamic polarization curves of SA-543 steel in different oil percentages with 0.01 M $\text{Na}_2\text{S}_2\text{O}_3 + \text{CO}_2$ solution at 25°C and 1 m/s.....	93
Figure 4.17	$R_p$ of SA-543 steel with time in 0.01 M $\text{Na}_2\text{S}_2\text{O}_3 + \text{CO}_2$ solution at different oil percentages. ....	93
Figure 4.18	Corrosion rate measurement of SA-543 and X65 steels at different oil percentages. ....	94

Figure 4.19	The potentiodynamic polarization curves of SA-543 steel in 0.01 M $\text{Na}_2\text{S}_2\text{O}_3$ + $\text{CO}_2$ solution with 30% oil at 25°C and different velocities. ....	96
Figure 4.20	$R_p$ of SA-543 steel with time in 0.01 M $\text{Na}_2\text{S}_2\text{O}_3$ + $\text{CO}_2$ solution with 30% oil at 25°C and different velocities.....	97
Figure 4.21	Corrosion rate measurement of SA-543 steel at different velocities.....	97
Figure 4.22	The potentiodynamic polarization curves of SA-543 steel in 0.01 M $\text{Na}_2\text{S}_2\text{O}_3$ + $\text{CO}_2$ solution with 30% oil at 1 m/s and different temperatures. ....	99
Figure 4.23	$R_p$ of SA-543 steel with time in 0.01 M $\text{Na}_2\text{S}_2\text{O}_3$ + $\text{CO}_2$ solution with 30% oil at 1 m/s and different temperatures. ....	99
Figure 4.24	Corrosion rate measurement of SA-543 steel at 1 m/s and different temperatures. ....	100
Figure 4.25	Vena contracta demonstration. ....	102
Figure 4.26	The potentiodynamic polarization curve for Exxsol D80 oil at 30% Oil and 70 % 0.01 M $\text{Na}_2\text{S}_2\text{O}_3$ . ....	103
Figure 4.27	Corrosion rate trend for Exxsol D80 oil at 30% Oil and 70% 0.01 M $\text{Na}_2\text{S}_2\text{O}_3$ . ....	103
Figure 4.28	Corrosion rate of D80 oil at different electrode positions. ....	104
Figure 4.29	The potentiodynamic polarization curve for Exxsol D80 and D130 oils at 30% Oil and 70% 0.01 M $\text{Na}_2\text{S}_2\text{O}_3$ . ....	106
Figure 4.30	Corrosion rate trend for Exxsol D80 and D130 oils at 30% Oil and 70% 0.01 M $\text{Na}_2\text{S}_2\text{O}_3$ . ....	108
Figure 4.31	Corrosion rate of D80 and D130 oils at different electrode positions.....	108



## LIST OF TABLES

Table 3.1 Chemical and physical properties of Exxsol D80 and D130 oils. ....	31
Table 3.2 Pumps specification. ....	43
Table 3.3 Flow-meter specification. ....	49
Table 3.4 Chemical Composition of SA-543 and X65 steels. ....	66
Table 3.5 Exposed area of test electrodes in different test sections. ....	70
Table 4.1 Tafel extrapolation data. ....	72
Table 4.2 Experimental series chart. ....	78
Table 4.3 Tafel extrapolation for different oil percentages ....	79
Table 4.4 Tafel extrapolation for different velocities. ....	82
Table 4.5 Tafel extrapolation for different temperatures. ....	85
Table 4.6 Tafel extrapolation for Na <sub>2</sub> S <sub>2</sub> O <sub>3</sub> and CO <sub>2</sub> . ....	89
Table 4.7 Tafel extrapolation for different oil percentages ....	92
Table 4.8 Tafel extrapolation for different velocities. ....	96
Table 4.9 Tafel extrapolation for different temperatures. ....	98
Table 4.10 Tafel extrapolation along the pipe length. ....	102
Table 4.11 Tafel extrapolation for different oils. ....	105

## LIST OF ABBREVIATIONS

$I_{\text{corr}}$	:	Corrosion current
$E_{\text{corr}}$	:	Corrosion potential
$\beta_a$	:	Anodic Tafel constant
$\beta_c$	:	Cathodic Tafel constant
$\text{Na}_2\text{S}_2\text{O}_3$	:	Sodium thiosulphate
$\text{CO}_2$	:	Carbon dioxide
O/W	:	Oil-in-water emulsion
W/O	:	Water-in-oil emulsion
$\text{H}_2\text{S}$	:	Hydrogen sulphide
$R_p$	:	Polarization resistance
$J_{\text{corr}}$	:	Current density
RCE	:	Rotating cylinder electrode
FAC	:	Flow accelerated corrosion

## ABSTRACT

**Full Name : Muhammad Nauman Zafar**

**Thesis title : H<sub>2</sub>S and CO<sub>2</sub> corrosion of SA-543 and X65 steels in oil/water emulsion corrosion**

**Major Field : Mechanical Engineering**

**Date of Degree : March, 2014**

An experimental study was performed using rotating cylinder electrode and a novel emulsion flow loop to investigate the corrosion behaviour of SA-543 and X65 steels when exposed to emulsion containing oil and sodium thiosulphate (Na<sub>2</sub>S<sub>2</sub>O<sub>3</sub>) solution along with carbon dioxide (CO<sub>2</sub>). This study aimed at understanding the effects of hydrodynamics on corrosion. Na<sub>2</sub>S<sub>2</sub>O<sub>3</sub> was used to generate the hydrogen sulphide (H<sub>2</sub>S). The emulsions were formed using 0.01 M Na<sub>2</sub>S<sub>2</sub>O<sub>3</sub> and Exxsol D80 oil. To mimic the well conditions, CO<sub>2</sub> was purged in order to maintain a pH of 5. Experiments were performed for different ranges of oil content, velocity, temperature, viscosity, and pipe diameter. Individual and combined effects of thiosulphate and CO<sub>2</sub> were also studied. It was observed that SA-543 steel was more corrosion resistant than X65 steel in the emulsion solution. Similar corrosion trend was found for both RCE and flow loop under the same test conditions. Iron sulphide film was formed on all the samples. Corrosion rates were reduced upon the introduction of CO<sub>2</sub> in the flowing fluid. The presence of oily phase dwindled the corrosion due to its inertness as oil is adsorbed on the steel surface. Increasing the velocity augmented the kinetics of reduction reaction thus forming sulphide film at higher rate and hence inhibiting the corrosion. Varying the temperature had a similar effect; corrosion dwindled by increasing the temperature due to the formation of stable sulphide films that are formed at higher temperatures. The corrosion

## الخلاصة

الاسم: محمد نعمان ظفر

عنوان الرسالة: تسبب كبريتيد الهيدروجين وثاني أكسيد الكربون في تآكل الفولاذ SA-543 و X65 في المستحلبات المائية / النفطية

التخصص الرئيسي: الهندسة الميكانيكية

تاريخ الدرجة العلمية: مارس 2014

تم إجراء دراسة تجريبية باستخدام قطب اسطواني دوار و جهاز تدفق حلقي جديد لم يتم استخدامه من قبل لدراسة سلوك تآكل الفولاذ SA-543 و X65 ، عند التعرض لمستحلب يحتوي على النفط ومحلول ثيوكبريتات الصوديوم ( $Na_2S_2O_3$ ) بالإضافة إلى ثاني أكسيد الكربون ( $CO_2$ ). وتهدف هذه الدراسة فهم آثار قوى الموائع على التآكل. وقد استخدم ثيوكبريتات الصوديوم لتوليد كبريتيد الهيدروجين ( $H_2S$ ). وتم تشكيل المستحلبات باستخدام 0.01 مل من ثيوكبريتات الصوديوم ( $Na_2S_2O_3$ ) ، و الزيت Exxsol D80. ولمحاكاة ظروف البئر تم إضافة ثاني أكسيد الكربون ( $CO_2$ ) من أجل الحفاظ على درجة 5 للأس الهيدروجيني. وقد أجريت التجارب على نطاقات مختلفة من محتوى الزيت ، والسرعة ، ودرجة الحرارة ، واللزوجة ، وقطر الأنبوب. وقد تم أيضا دراسة التأثير الفردي و الجماعي للثيوكبريتات وثاني أكسيد الكربون. ولوحظ أن فولاذ SA-543 كان أكثر مقاومة للتآكل من فولاذ X65 في محلول المستحلب. وقد تبين وجود نفس سلوك التآكل في كل من القطب الاسطواني الدوار و جهاز التدفق الحلقي في ظل نفس ظروف الإختبار. وتشكلت طبقة من كبريتيد الحديد على جميع العينات. وظهر تثبيط أكثر في عملية التآكل في التجارب التي تم إضافة ثاني أكسيد الكربون إليها. و أدى وجود الزيت إلى تضاءل التآكل بسبب وجود طبقة من الزيت على سطح الفولاذ. وتسببت زيادة السرعة في زيادة حركية تفاعل الاختزال وبالتالي تشكلت طبقة من الكبريتيد بمعدل أعلى مما ثبت التآكل. وقد كان لتغيير درجة الحرارة تأثير مماثل ، حيث تضاءل التآكل مع زيادة درجة الحرارة بسبب تشكل طبقات مستقرة من الكبريتيد والتي تتشكل عند درجات الحرارة العالية. وكان معدل التآكل في العينة الموجودة بالقرب من مدخل قناة الإختبار أكثر من العينة الموجودة بالقرب من مخرج قناة الإختبار بسبب زيادة الاضطرابات التدفقية عند المدخل. وأدت الزيادة في لزوجة النفط إلى الزيادة في معدل التآكل وذلك بسبب ارتفاع إجهادات القص.

## درجة الماجستير في العلوم

جامعة الملك فهد للبترول والمعادن

الظهران - المملكة العربية السعودية

# CHAPTER 1

## INTRODUCTION

### 1.1 Introduction

Corrosion is defined as the degradation of metals through electrochemical processes. Losses due to corrosion are worth multi-billion dollars, with an estimated figure of \$200 billion per year [1]. Corrosion has to occur as every element has tendency to go back to its stable state. One can not eliminate corrosion but can take measures to slow down the corrosion process. Corrosion of materials poses threat to plant safety and also affects the smoothness of production process. Corrosion is further classified according to the media they are exposed to, either it is dry or wet corrosion. There are multiple types of corrosion, but we will mainly focus on flow accelerated corrosion. This type of corrosion depends highly on flow conditions. In flow accelerated corrosion, the scale on the surface is eroded by the flow and thus exposing the bare metal to corrosion.

Flow in petrochemical, pharmaceutical, and process industries is usually a multiphase flow. Multiphase flow means that two or more phases are flowing at a moment. The characteristics of multiphase flow are different from single phase flow. Multiphase flow has certain flow patterns which are formed according to the two fluid velocities. Emulsion is a sort of multiphase flow, but the difference is that emulsions are formed by agitation. Emulsion exists in a metastable state, formed by mechanical agitation and the presence of surfactant molecules that diminish interfacial tension [2]. If you flow two fluids with different densities, they will remain separated during the flow. In case of emulsion, they will be usually mixed up. Emulsion is a mixture of two or more fluids that

are immiscible and remain suspended as dispersed particles. They are further classified into two types. i.e. i) Oil-in-water emulsion (O/W), ii) Water-in-oil emulsions (W/O). Their classification is dependent upon the dispersed phase. When oil is dispersed in water phase, this is known as oil-in-water emulsion and when water particles are dispersed in oil phase it is known as water-in-oil emulsions. The properties of the above two mentioned emulsions are different from each other. The type of emulsion is dependent on the fraction of one fluid into the other.

Emulsions are one of the essentials of our life, ranging from foods, cosmetics, pesticides, medicines, paints etc. Emulsions are usually formed to ease the extraction of oil and on the other hand emulsions form at the valves, flanges poses threat to the life of equipment. The corrosion and mechanical properties of emulsion are different from their constituent fluids. Emulsion corrosion has been observed to have higher corrosion rate as compared to individual oil water corrosion [3]. In this study we will mainly focus on oil-in-water emulsion, where water is present as a continuous phase; metallic corrosion is expected due to water. Since oil is known to wet metals, the destabilization of the emulsion at the interface could significantly alter the corrosion behaviour compared with aqueous water phase alone [4,5]. The corrosion rate may be affected also by changes in the rate of transport of oxygen from reactants to the metal surface, as a result to the presence of oil in the system [2,6-9].

CO<sub>2</sub> and H<sub>2</sub>S gases are type of gases that exist in crude oil wells. Both gases form acids when combined with moisture. Corrosion due to CO<sub>2</sub> is known as sweet corrosion and sour corrosion is due to H<sub>2</sub>S. The extraction of oil from sour wells is relatively expensive due to the higher refining costs in removing sulphur. But the high oil demands make the

extraction of H<sub>2</sub>S containing oil highly essential. H<sub>2</sub>S is a toxic gas with a rotten egg smell, and its exposure up to 15 ppm is considered hazardous. It is a poisonous, corrosive, heavier than air, and explosive gas [10]. H<sub>2</sub>S is known to cause stress corrosion cracking (SCC) due to the brittlement of material via hydrogen ingress [11,12]. Corrosion in sour environment is usually initiated with the formation of iron sulphide film [11]. Iron sulphide scales are usually formed inside the sour well pipelines, and observed to have both corrosive and inhibitive properties. The film formation depends on temperature, where stable adherent films are formed at higher temperatures (> 80°C) [11,13].

In petroleum industry, the sulphur present in sour crude oil, which is sometimes used as a feedstock for hydrocrackers, produces iron sulphide scale. The scale subsequently reacts with water and oxygen during shutdowns to form polythionic acids (H<sub>2</sub>S<sub>x</sub>O<sub>6</sub>) and other oxyanions such as thiosulphate (S<sub>2</sub>O<sub>3</sub><sup>2-</sup>). Analogies have been established between polythionic acid cracking, where the most aggressive sulphur species is considered to be S<sub>4</sub>O<sub>6</sub>, and SCC in thiosulphate solution [14].

Corrosion due to CO<sub>2</sub> is known as sweet corrosion as it has no smell. CO<sub>2</sub> forms weak acid in aqueous media which causes internal corrosion in oil/gas pipelines. CO<sub>2</sub> has certain advantages along with its some detrimental effects. CO<sub>2</sub> is injected into the well to reduce the viscosity of oil and to increase the production of well [15-17]. This process is known as enhanced oil recovery. CO<sub>2</sub> corrosion usually involved the formation of iron carbide (Fe<sub>3</sub>C) and iron carbonate (FeCO<sub>3</sub>) with the evolution of H<sub>2</sub>. Corrosion is substantially reduced when FeCO<sub>3</sub> is precipitated on the steel surface due to its dense and protective corrosion product film which acts as a diffusion barrier for corrosive species to travel to metal surfaces [15,18]. The nature of carbonate film is dependent upon alloy,

temperature, CO<sub>2</sub> partial pressure, and pH [19-25]. The increase in pH favors the formation of FeCO<sub>3</sub>.

A new approach has been adapted in this research by using sodium thiosulphate (Na<sub>2</sub>S<sub>2</sub>O<sub>3</sub>) instead of H<sub>2</sub>S, since H<sub>2</sub>S is a toxic and flammable gas, and requires special safety measures for its usage. This replacement made the study of H<sub>2</sub>S effects at laboratory scale practically feasible. Thiosulphate is a non-toxic anion and found to be a good substituent for H<sub>2</sub>S. This idea was first proposed by Tsujikawa et al. [26] where he used sodium thiosulphate for stress corrosion cracking of low alloy steels. The results were in good agreement with the solutions containing H<sub>2</sub>S. S<sub>2</sub>O<sub>3</sub><sup>2-</sup> being metastable anion reduces to form H<sub>2</sub>S gas at the metal surface. This reaction is spontaneous at open circuit potential of steel [11]. The exact disproportion reaction of thiosulphate is still ambiguous, but it is believed that the reduction of thiosulphate anion produces elemental sulphur and this elemental sulphur further combines with proton to form H<sub>2</sub>S [11,15,27]. The formation of FeS on the surface is done from both elemental sulphur and H<sub>2</sub>S. Mackinawite (FeS) is formed initially on the metal surface because the kinetics of Mackinawite formation are faster than any other FeS species [15,28-31]. This surface is loose, less adherent and rich in defects which contributes to good electron conductivity and sometimes also inhibits the anodic dissolution by hindering the movement of iron ions [11,15,32]. The formation of sulphide film on surface is dependent upon pH; with an increase in pH, the solubility of sulphide film is reduced, and the maximum sulphide precipitation occurs at pH 4. However the amount of mackinawite augments with time due to high stability [11].



Kappes et al. [27,33] quoted in his study that the H<sub>2</sub>S generation rate was maximum for the 0.01 M Na<sub>2</sub>S<sub>2</sub>O<sub>3</sub>. Increasing the concentration resulted in reducing the H<sub>2</sub>S generation rate due to thick formation of sulphide film. The sulphide film was good catalyst for cathodic reactions. The film growth rate was also higher in thiosulphate solutions as compared to H<sub>2</sub>S containing solutions [11].

Pipelines at oil and gas facilities are affected by flow accelerated corrosion (FAC). FAC results in totally or partially removal of protective surface films and higher wear rate resulting in thinning of pipelines [34]. Most affected piping components by FAC are usually sudden expansion or contraction, orifice, valves, tees, elbows. This is due to severe changes in flow direction as well as the development of secondary flow instabilities downstream of these components [34-36]. The changes in fluid hydrodynamics, turbulence, wall shear stress, the formation and destruction of corrosion product film are all related to hydrodynamic boundary layer in the vicinity of metal substrate [37].

Increasing demands leads to an increase in productions, and the increase in production requires high strength corrosion resistant materials in order to reduce the maintenance downtime. SA-543 is a high strength quenched and tempered steel. It is recently introduced in the construction of reactors in petrochemical plants. Usage of these types of materials will reduce the corrosion allowance to the wall and, reducing weight and increasing the capacity of equipment. SA-543 comprises of nickel, chromium and molybdenum. These three elements provide high corrosion resistance and enhance the performance. Chromium helps in formation of highly corrosion resistant stable oxide layer and molybdenum is used to augment pitting and crevice corrosion resistance [38].

## **1.2 Thesis objective**

The main objective of this thesis is to investigate the corrosion of SA-543 and X65 steels in hydrodynamic H<sub>2</sub>S and CO<sub>2</sub> environments. Initial study will be performed using rotating cylinder electrode with oil/water emulsion. The emulsion corrosion will be studied for different oil percentages, velocities and temperatures. Once the trend of emulsion corrosion will be at hand, similar experiments will be performed using emulsion flow loop. Using flow loop, the effect of viscosity, pipe diameter, and corrosion along the length of vertical pipe will be investigated. Finally, a comprehensive analysis will be given for the above two techniques.

## **1.3 Thesis structure**

This thesis is splitted into 5 chapters started with introduction in which a brief introduction on emulsion, CO<sub>2</sub> and H<sub>2</sub>S corrosion are highlighted. The second chapter provides a comprehensive literature review on emulsion corrosion, H<sub>2</sub>S and CO<sub>2</sub> corrosion, using RCE and flow loop, with some of the renowned institutes that are working on erosion-corrosion. Third chapter comprises of a description for the rotating cylinder electrode setup and flow loop setup. Results and discussion is given in chapter four. At the end of thesis conclusions were listed in chapter 5 with some recommendations followed by references.

## CHAPTER 2

### LITERATURE REVIEW

A thorough literature survey was performed ranging from the H<sub>2</sub>S and CO<sub>2</sub> corrosion in multiphase to the discovery of thiosulphate as H<sub>2</sub>S replacement. Each aspect of Na<sub>2</sub>S<sub>2</sub>O<sub>3</sub> and CO<sub>2</sub> corrosion were meticulously gathered. The effect of pipe diameters, inlet sharpness, contraction, expansion, each and every aspect of pipeline corrosion was reviewed. This literature review is divided into two sections; first section deals with the published literature, and the second section highlights the current multiphase corrosion facilities around the globe.

#### 2.1 Literatures

##### 2.1.1 H<sub>2</sub>S and CO<sub>2</sub> corrosion

Hamzah et al. [39] setup an experimental test for the erosion-corrosion of C-Mn steel. This steel is heavily used in petroleum industry. The C-Mn was tested with wet and dry carbon dioxide conditions with varying impact angles and insertion of sand particles. Material loss was augmented with the insertion of sand particles. For velocities below 50 m/s the erosion was dominated by scale setup and its removal and by substrate erosion for velocities greater than 50 m/s. The ferric carbonate scale formed due to wet carbon dioxide is weak in strength at temperature between 20 - 80°C.

Perdomo et al. [40] studied the corrosion of API 5LB and X52 steels at both field level and laboratory scale when they are exposed to Furrial's crude oil from different wells in presence of H<sub>2</sub>S and CO<sub>2</sub>. The experiments were performed for different water cuts. The corrosion rates for both materials were almost the same with corrosion resistance of X52

steel being slightly greater. This higher resistance could be due to higher content of sulphur and manganese as compared to the API 5LB steel. Pitting on the materials was significant. Higher water cuts yielded higher corrosion and oil showed its natural inhibiting properties at low water cuts.

Ma et al. [41] studied the influence of  $H_2S$  on carbon steels using electrochemical impedance under varying conditions of pH,  $H_2S$  concentration and exposure time. By increasing the pH from 0.75 to 3.5, the charge transfer resistance was increased, which depicts the formation of inhibition sulphide film. When the specimen was exposed to higher exposure time ( $> 2hr$ ) the probability of formation of sulphide film increased.  $H_2S$  augmented both the anodic and cathodic reactions. The sulphide films transforms from loose mackinawite film to firm and stable pyrite film with the passage of time.

Lee and Netic [42,43] studied the effect of  $H_2S$  and  $CO_2$  corrosion using impedance spectroscopy method. In Nyquist plots depressed semi-circles were found which suggested that the film formed on the surface was heterogeneous and rough and caused the non-uniform distribution of current density on the surface. Thin film of sulphide was rapidly formed on the surface and was reportedly classified as Mackinawite ( $FeS$ ). Polarization resistance increased with time specifying the formation of film on the surface.

Brown and Netic [44] highlighted the importance of scale forming on  $H_2S$  and  $CO_2$  corrosion. The formation of mackinawite reduced the corrosion rate in all experiments. The precipitation values of iron carbonate and iron sulphide played a key role in

augmenting the corrosion values. The film composed of multi-layers in presence of carbon dioxide and hydrogen sulphide.

Fang et al. [45] studied the concentration effect of NaCl on corrosion. It was observed that the increasing the concentration of NaCl reduced the CO<sub>2</sub> corrosion rate as the salt slow down the anodic and cathodic reactions. Presence of high concentration of salt reduced the cathodic charge transfer reaction. Velocity didn't have any significant effect on corrosion at higher salinity concentrations.

Sun et al. [30] studied the kinetics of the scale formed in the presence of CO<sub>2</sub> and H<sub>2</sub>S. The rate of precipitation of CO<sub>2</sub> was function of iron carbonate super saturation, solubility, temperature and surface area to volume ratio. For X65 steel using H<sub>2</sub>S the corrosion rate increased initially but declined as the time proceed. The formation of Mackinawite was dominant and increased with H<sub>2</sub>S concentration, but long exposures resulted in reduction in thickness. The precipitate of iron carbonate along with Mackinawite was only found for 0.1% H<sub>2</sub>S and 50 ppm of Fe<sup>2+</sup> concentrations. Corrosion rate was seen to be dependent upon the rate of scale precipitation.

Fang et al. [46] investigated the effect of elemental sulphur on corrosion. Elemental sulphur is usually formed by the contamination of hydrogen sulphide. Acidification reaction with water was observed at temperature higher than 80°C. It was confirmed that the iron sulphide scale formed is mackinawite. The scale thickened as the time progressed. Localized corrosion was more pronounced.

Han et al. [47] conducted his study on the passive films that are formed in CO<sub>2</sub> environments on mild steel. Experiments were performed at 80°C, 0.53 bar CO<sub>2</sub> pressure

H2S AND CO2 CORROSION OF SA-543 AND X65 STEELS IN OIL /WATER EMULSION	العنوان:
Zafar, Muhammad Nauman	المؤلف الرئيسي:
-Al Hadhrami, Luai Muhammad, Rihan, Rihan O.(Advisor, Co Advisor)	مؤلفين آخرين:
2014	التاريخ الميلادي:
الظهران	موقع:
1 - 121	الصفحات:
651787	رقم MD:
رسائل جامعية	نوع المحتوى:
English	اللغة:
رسالة ماجستير	الدرجة العلمية:
جامعة الملك فهد للبترول والمعادن	الجامعة:
عمادة الدراسات العليا	الكلية:
السعودية	الدولة:
Dissertations	قواعد المعلومات:
التآكل، الصلابة، الهندسة الميكانيكية	مواضيع:
<a href="https://search.mandumah.com/Record/651787">https://search.mandumah.com/Record/651787</a>	رابط:

**H<sub>2</sub>S AND CO<sub>2</sub> CORROSION OF SA-543 AND X65**

**STEELS IN OIL/WATER EMULSION**

BY

**MUHAMMAD NAUMAN ZAFAR**

A Thesis Presented to the  
DEANSHIP OF GRADUATE STUDIES

**KING FAHD UNIVERSITY OF PETROLEUM & MINERALS**

DHAHRAN, SAUDI ARABIA

1963 ١٣٨٣

In Partial Fulfillment of the  
Requirements for the Degree of

**MASTER OF SCIENCE**

In

**MECHANICAL ENGINEERING**

**MARCH 2014**